JACS
JOURNAL OF THE AMERICAN CHEMICAL SOCIETY

ARTICLE

pubs.acs.org/JACS

Intriguing Interconnections Among Phase Transition, Magnetic Moment, and Valence Disproportionation in 2H-Perovskite Related Oxides

Qingbiao Zhao,[†] Jacques Darriet,[‡] Myung-Hwan Whangbo,[°] Longfei Ye,[§] Chavis Stackhouse,[†] and Hans-Conrad zur Loye*[,†]

[†] Department of Chemistry and Biochemistry, University of South Carolina, Columbia, South Carolina 29208, United States

[‡] Institut de Chimie de la Matière Condensée de Bordeaux (ICMCB-CNRS-Université Bordeaux I), 87 Avenue du Dr. Schweitzer, 33608 Pessac Cedex, France

[°] Department of Chemistry, North Carolina State University, Raleigh, North Carolina 27695, United States

[§] Department of Physics and Astronomy, University of South Carolina, Columbia, South Carolina 29208, United States

ABSTRACT: In this paper we report the crystal growth, structure determination, and magnetic properties of the 2H-perovskite related oxides, $Sr_5Co_4O_{12}$ and $Sr_6Co_5O_{15}$, as well as the charge disproportionation and associated phase transition of $Sr_5Co_4O_{12}$. $Sr_5Co_4O_{12}$ and $Sr_6Co_5O_{15}$ are the ($m = 2$, $n = 3$) and ($m = 1$, $n = 1$) members of the $A_{3m+3n}A'_nB_{3m+n}O_{9m+6n}$ family, respectively. $Sr_6Co_5O_{15}$ crystallizes in the space group $R32$ with lattice parameters of $a = 9.5020(10)$ Å and $c = 12.379(8)$ Å. The structure solution shows that $Sr_6Co_5O_{15}$ is isostructural with $Sr_6Rh_5O_{15}$. Magnetic measurements do not indicate any long-range magnetic order, although the Weiss temperature of −248 K indicates the presence of dominant antiferromagnetic interactions. $Sr_5Co_4O_{12}$ crystallizes in the space group $P\text{-}3c1$ with lattice parameters of $a = 9.4705(10)$ Å and $c = 20.063(5)$ Å at room temperature. The single crystal structure solution revealed that the cobalt ions in the trigonal prismatic sites of $Sr_5Co_4O_{12}$ undergo a structural transition at ~170 K, where the cobalt atoms are in the center of the trigonal prisms below this temperature and move partially toward the faces above this temperature. This structure transition is accompanied by a change in the magnetic moment of the oxide and can be related to a valence disproportionation of the cobalt ions and a concomitant Jahn−Teller distortion. In addition, specific heat, Seebeck coefficient, electric conductivity, and magnetic measurements as well as bond valence sum calculations were carried out for $Sr_5Co_4O_{12}$. $Sr_5Co_4O_{12}$ exhibits strong magnetic anisotropy but no long-range magnetic order.

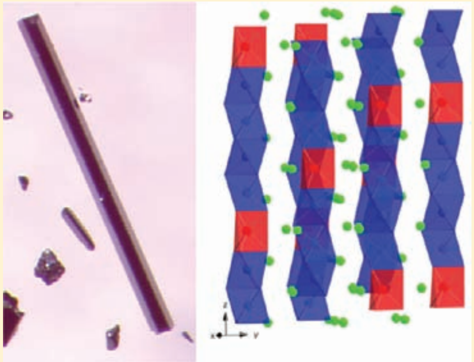

INTRODUCTION

The ABO_3 perovskite family of oxides is perhaps the most studied family of oxides due to the diverse properties exhibited by different members, including complex magnetic phenomena, superconductivity, ferroelectricity, and ionic conductivity, to mention a few.[1] Thus it is not surprising that different approaches to describe the perovskite structure have been developed over the years to support the specific aspect one wishes to emphasize.[2] For example, the ideal cubic perovskite structure, ABO_3, can be described as consisting of corner-sharing BO_6 octahedra with the A cations occupying the 12-coordinate site in the middle of a cube formed by eight such BO_6 octahedra. Numerous structural variants exist due to the size limitations between the A and the B cations, which lead to the tilting of the octahedra within the cubic perovskite structure if A is "too small" for B, or to the hexagonal variant consisting of infinite chains of face-sharing BO_6 octahedra if A is "too large" for B.[3]

Another approach to describing both the cubic and the hexagonal perovskite structures is based on the stacking of close-packed $[AO_3]$ layers and the subsequent filling of the generated octahedral sites by the B cations. If the $[AO_3]$ layers are stacked in an ABC fashion then the cubic perovskite structure results, while an AB stacking sequence of $[AO_3]$ layers results in the hexagonal (2H) perovskite structure. A complex variant of the 2H-perovskite structure in oxides was discovered by Randall and Katz[4] when they prepared Sr_4PtO_6, which contains trigonal prisms in addition to octahedra in the chains. This was the first example of a large series of oxides referred to as *2H-perovskite related oxides* and the title compounds fall into this group.

The structures of the 2H-perovskite related oxides are best thought of as resulting from the stacking of A_3O_9 and $A_3A'O_6$ layers and the subsequent filling of the generated octahedral sites by the B cations, as first proposed by Darriet et al.[5] The $A_3A'O_6$ layer is generated by substituting one A′ cation for 3 oxygen atoms in an A_3O_9 (tripled AO_3) layer. Stacking of m A_3O_9 and n $A_3A'O_6$ layers and filling of the octahedral sites by the B cations generates the structures of a series of oxides with the general

Received: October 4, 2011
Published: December 05, 2011

ACS Publications © 2011 American Chemical Society

dx.doi.org/10.1021/ja209198b | J. Am. Chem. Soc. 2011, 133, 20981–20994

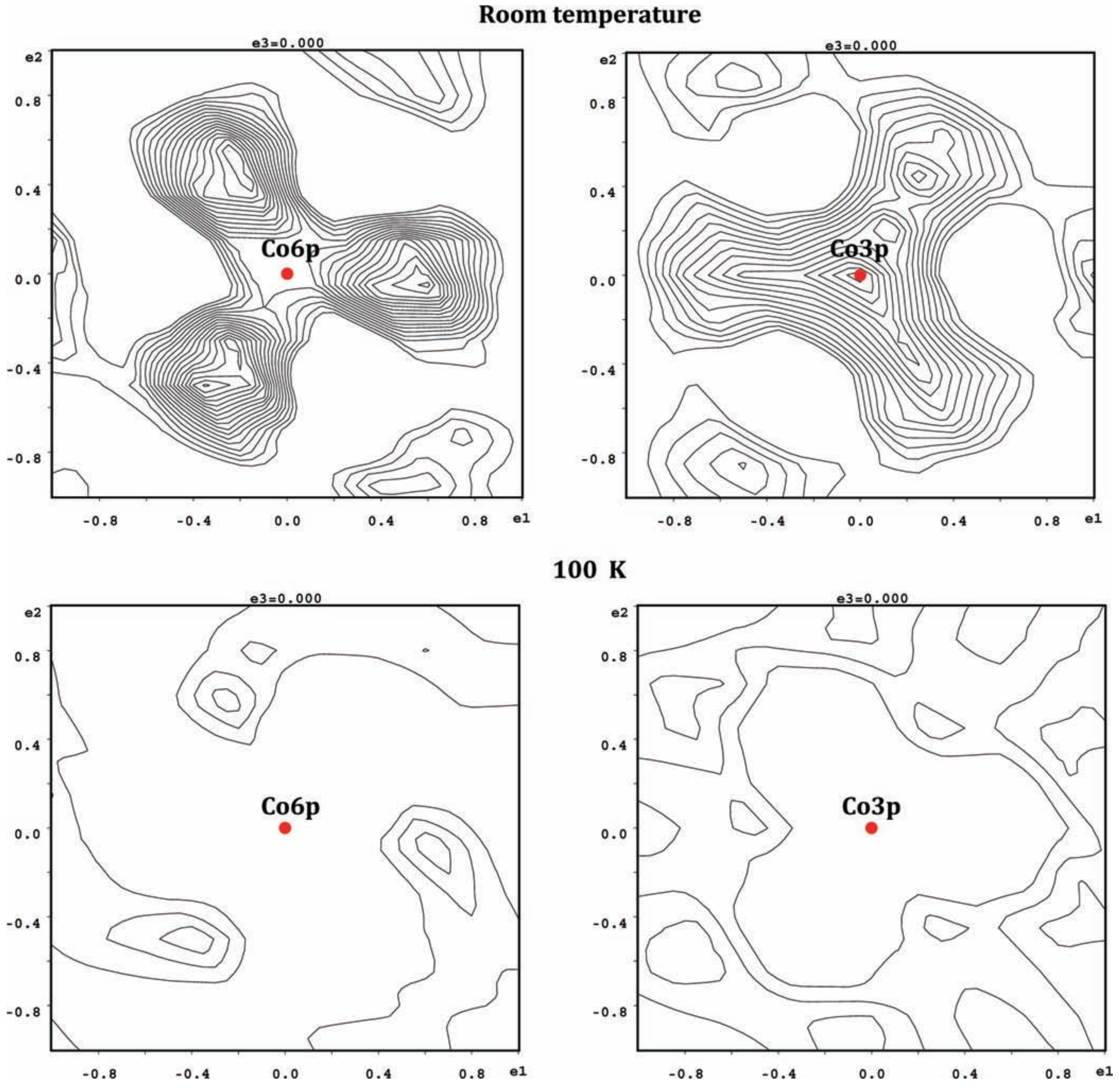

Figure 1. Difference Fourier maps around Co3p and Co6p prismatic sites. At room temperature, (top two Fourier maps), Co are partially off center, while at 100 K (bottom two Fourier maps), Co atoms occupy only the center of the trigonal prisms. Contour lines in interval of 0.2 Å^{-3}.

formula $A_{3m+3n}A'_nB_{3m+n}O_{9m+6n}$.[6] The 2H-perovskite related structure contains infinite chains made up of face-sharing BO_6 octahedra and $A'O_6$ trigonal prisms. The octahedra and trigonal prisms are typically slightly distorted via a twist around the chain axis. A thorough description of the structures was given by Perez-Mato et al.,[7] and the compositions and properties were reviewed by Stitzer et al.[6] and zur Loye et al.[8]

The A cation in the $A_{3m+3n}A'_nB_{3m+n}O_{9m+6n}$ family is typically an alkaline earth, although recently compositions with mixed lanthanide-alkali metals have been reported,[9] while the A′ and B cations can be an alkali, alkaline-earth, main group, or rare-earth metal in oxidation states ranging from +1 to +5. This extended family of 2H-perovskite related oxides has attracted extensive interest both for its structural diversity due to the many possible repeat sequences of the A_3O_9 and $A_3A'O_6$ layers, and accordingly, different repeat sequences of face-sharing octahedra and trigonal prisms[5−7,10] as well as for the diverse physical properties that have been observed.[11,12]

Compositions containing cobalt and rhodium have been extensively investigated as both of these metals are readily incorporated into this structure, where they can be found in oxidation states ranging from +3 to +5. The $Ca_3Co_2O_6$ composition is perhaps the most studied 2H-perovskite related oxide,[13,14] partially because it has interesting magnetic[15,16] and thermoelectric[12,17]

Table 1. Crystallographic Data for $Sr_5Co_4O_{12}$ at Room Temperature, $Sr_5Co_4O_{12}$ at 100 K, and $Sr_6Co_5O_{15}$ at Room Temperature

	$Sr_5Co_4O_{12}$ (293 K)	$Sr_5Co_4O_{12}$ (100 K)	$Sr_6Co_5O_{15}$ (293 K)
formula	$Sr_5Co_4O_{12}$	$Sr_5Co_4O_{12}$	$Sr_6Co_5O_{15}$
formula weight (g/mol)	865.83	865.83	1060.38
wavelength	Mo$K\alpha$ (0.71073 Å)	Mo$K\alpha$ (0.71073 Å)	Mo$K\alpha$ (0.71073 Å)
crystal system	trigonal	trigonal	trigonal
space group	*P*-3*c*1	*P*-3*c*1	*R*32
cell parameters	a = 9.4705(10) Å	a = 9.4461(10) Å	a = 9.5020(10) Å
	b = 9.4705(10) Å	b = 9.4461(10) Å	b = 9.5020(10) Å
	c = 20.063(5) Å	c = 20.0168(5) Å	c = 12.379(8) Å
	α = 90°	α = 90°	α = 90°
	β = 90°	β = 90°	β = 90°
	γ = 120°	γ = 120°	γ = 120°
volume (Å^3)	1558.3(5)	1546.79(5)	967.9(7)
Z	6	6	3
calculated density (g/cm^3)	5.534	5.575	5.456
linear absorption coefficient (mm^{-1})	31.74	31.98	30.92
twin matrices			
F(000)	2364	2364	1448
$\sin(\theta/\lambda)_{max}$	0.81	0.81	0.91
hkl ranges	$-15 < h < 15, -15 < k < 15, -32 < l < 32$	$-15 < h < 15, -15 < k < 15, -32 < l < 32$	$17 < h < 17, -17 < k < 17, -22 < l < 22$
number of reflections	57871	65075	38195
number of independent reflections	2300	2282	2235
R_{int}	0.244	0.022	0.189
absorption correction	Gaussian	Gaussian	Gaussian
T_{min}, T_{max}	0.010, 0.108	0.013, 0.107	0.079, 0.868
refinement method	F^2	F^2	F^2
$R(F)$	0.0352 (nonharmonic model), 0.0355 (splitting model)	0.0385	0.0418
$wR(F^2)$	0.0911 (nonharmonic model), 0.0920 (splitting model)	0.0986	0.0745
$(\Delta/\sigma)_{max}$	0.011 (nonharmonic model), 0.0007 (splitting model)	0.0004	0.0003

properties. Similarly other cobalt containing compositions have been studied, including $Sr_6Co_5O_{15}$, which was synthesized as a polycrystalline powder and whose structure was determined using powder neutron diffraction data.[18] Oxygen deficient and incommensurate $Sr_5Co_4O_{12-\delta}$ crystals were synthesized and can become oxygen stoichiometric and commensurate upon annealing; in addition, oxygen excess $Sr_6Co_5O_{15+\delta}$ was reported in the same study. These samples were characterized with SAED, TEM, and HRTEM, but no atomic coordinates were provided.[19] Other researchers pursued the powder synthesis of additional cobalt compositions including $(Sr_{0.5}Ca_{0.5})_4Co_3O_9$, $Sr_5Co_4O_{12}$, and $(Sr_{1-x}Ba_x)_6Co_5O_{15}$, which were synthesized and characterized by HRTEM and SAED. Only the atomic coordinates of $Sr_5Co_4O_{12}$ were given,[20] which however are unlikely to be correct (see below). More complicated compositions like $(Ca_{0.4}Sr_{0.6})_9Co_7O_{21}$, $Sr_{14}Co_{11}O_{33}$, $Sr_{21}Co_{17}O_{51}$, and $Ba_{66}Co_{59}O_{177}$ were reported and characterized with SAED and HRTEM. However, here also, no atomic coordinates were provided.[21] $Sr_6Rh_5O_{15}$, isostructural with $Sr_6Co_5O_{15}$, was first grown in single crystal form by Stitzer et al. who determined the single crystal structure and thoroughly investigated the highly anisotropic magnetic properties.[11] Crystals with larger repeating sequences of polyhedra, like $Ba_9Rh_8O_{24}$, $Ba_{11}Rh_{10}O_{30}$, and $Ba_{32}Rh_{29}O_{87}$, were also grown by Stitzer et al. and were structurally and magnetically characterized.[11,22] These structure solutions were used by Sun et al. as a starting point for solving the structures of single crystals of oxygen deficient $Sr_6Co_5O_{15-\delta}$.[23] As the polyhedral repeat sequence is highly sensitive to the oxygen content, it was not surprising that the oxygen deficient structures were incommensurate and the structure solutions obtained via the 4-D superspace group approach did not match that of $Sr_6Rh_5O_{15}$.

The ability to grow single crystals[24] of these 2H-perovskite related oxides was an important breakthrough as it enabled the structure determination of many new compositions and allowed for the determination of the anisotropic magnetic properties using oriented single crystals. However, even the single crystal growth of this group of oxides has its challenges, and many crystals are incommensurate.[19,25,26] Herein we report the hydroxide flux growth of high quality commensurate single crystals of $Sr_5Co_4O_{12}$ and $Sr_6Co_5O_{15}$ and describe the structure determination and their physical properties, including an intriguing phase transition in $Sr_5Co_4O_{12}$ that is accompanied by a change in the magnetic moment, which can be correlated with a charge disproportionation of the cobalt ions in the trigonal prismatic sites.

Table 2. Fractional Atomic Coordinates and Equivalent Isotropic Parameters[a] (Å^2) for $Sr_5Co_4O_{12}$ at Room Temperature with Nonharmonic Model, at Room Temperature with Split Model, and at 100 K and $Sr_6Co_5O_{15}$ at Room Temperature

		$Sr_5Co_4O_{12}$ (Room Temperature, Nonharmonic Model)				
atom	Wyckoff position	*x*	*y*	*z*	*Ueq*/**Uiso*	occupancy
Sr1	12*g*	0.00751(14)	0.34354(9)	0.14874(2)	0.0134(3)	
Sr2	12*g*	0.30449(8)	0.33246(14)	0.04862(2)	0.0070(2)	
Sr3	6*f*	0.35678(7)	0.35678	1/4	0.0074(3)	
Co1	2*b*	0	0	0	0.0029(4)	
Co2	4*c*	0	0	0.12227(7)	0.0052(3)	
Co3p	2*a*	0	0	1/4	0.0112(3)	
Co4	4*d*	1/3	2/3	0.08401(7)	0.0047(3)	
Co5	4*d*	1/3	2/3	0.20382(8)	0.0034(2)	
Co6p	4*d*	1/3	2/3	0.45639(14)	0.0234(4)	
Co7	4*d*	1/3	2/3	0.32554(7)	0.0057(3)	
O1	12*g*	0.4888(5)	0.8215(7)	0.1448(2)	0.0064(15)	
O2	12*g*	0.3258(6)	0.8194(5)	0.26322(15)	0.0065(14)	
O3	12*g*	0.1664(5)	0.0188(5)	0.06030(19)	0.0076(13)	
O4	12*g*	0.1729(6)	0.6579(5)	0.52544(12)	0.0099(15)	
O5	12*g*	0.1838(9)	0.6687(7)	0.3836(2)	0.033(3)	
O6	12*g*	0.1601(6)	0.1295(6)	0.3176(2)	0.027(2)	

		$Sr_5Co_4O_{12}$ (Room Temperature, Split Model)				
atom	Wyckoff position	*x*	*y*	*z*	*Ueq*/**Uiso*	occupancy
Sr1	12*g*	0.00744(14)	0.34359(9)	0.14874(2)	0.0133(3)	
Sr2	12*g*	0.30445(8)	0.33242(14)	0.04862(2)	0.0079(2)	
Sr3	6*f*	0.35677(7)	0.35677	1/4	0.0074(2)	
Co1	2*b*	0	0	0	0.0026(4)	
Co2	4*c*	0	0	0.12222(7)	0.0052(3)	
Co3p	2*a*	0	0	1/4	*0.0114(7)	0.996(6)
Co3	6*f*	0	0.069(119)	1/4	*0.0114(4)	0.004
Co4	4*d*	1/3	2/3	0.08392(7)	0.0047(3)	
Co5	4*d*	1/3	2/3	0.20380(7)	0.0044(1)	
Co6p	4*d*	1/3	2/3	0.4562(2)	*0.0110(6)	0.689(6)
Co6	12*g*	0.372(2)	0.665(2)	0.4554(5)	*0.0110(6)	0.311
Co7	4*d*	1/3	2/3	0.32543(7)	0.0059(3)	
O1	12*g*	0.4888(5)	0.8214(3)	0.1449(2)	0.007(2)	
O2	12*g*	0.3260(6)	0.8195(5)	0.26324(15)	0.0063(14)	
O3	12*g*	0.1664(5)	0.0188(3)	0.0603(2)	0.0079(13)	
O4	12*g*	0.1728(3)	0.6580(7)	0.5261(2)	0.0101(15)	
O5	12*g*	0.1834(9)	0.6680(4)	0.3835(2)	0.033(3)	
O6	12*g*	0.1601(6)	0.1294(6)	0.3177(2)	0.027(2)	

		$Sr_5Co_4O_{12}$ (100 K)				
atom	Wyckoff position	*x*	*y*	*z*	*Ueq*/**Uiso*	occupancy
Sr1	12*g*	0.00736(12)	0.34298(8)	0.14892(2)	0.0082(2)	
Sr2	12*g*	0.30459(8)	0.33335(11)	0.04833(2)	0.0030(2)	
Sr3	6*f*	0.35712(6)	0.35712	1/4	0.0033(2)	
Co1	2*b*	0	0	0	0.0009(4)	
Co2	4*c*	0	0	0.12186(7)	0.0026(3)	
Co3p	2*a*	0	0	1/4	0.0112(3)	
Co4	4*d*	1/3	2/3	0.08386(7)	0.0024(4)	
Co5	4*d*	1/3	2/3	0.20379(8)	0.0018(2)	
Co6p	4*d*	1/3	2/3	0.45563(8)	0.0108(3)	
Co7	4*d*	1/3	2/3	0.32531(6)	0.0036(3)	
O1	12*g*	0.1774(4)	0.6671(6)	0.1452(2)	0.0053(14)	

Table 2. Continued

$Sr_5Co_4O_{12}$ (100 K)						
atom	Wyckoff position	*x*	*y*	*z*	*Ueq/*Uiso*	occupancy
O2	12*g*	0.3250(6)	0.8198(5)	0.2630(16)	0.0032(13)	
O3	12*g*	0.1472(4)	0.1656(4)	0.9402(2)	0.0031(11)	
O4	12*g*	0.3426(6)	0.8270(5)	0.0249(2)	0.0063(14)	
O5	12*g*	0.3306(8)	0.5169(6)	0.3840(2)	0.023(2)	
O6	12*g*	0.1310(5)	0.1607(5)	0.1828(2)	0.019(2)	

$Sr_6Co_5O_{15}$ (Room Temperature)						
atom	Wyckoff position	*x*	*y*	*z*	U_{eq}/**Uiso*	occupancy
Co1		0	0	0.90367	0.00549(17)	
Co2		0	0	0.7068	0.0078(2)	
Co3		0	0	0.5	0.0166(4)	
O1		0.1604	0.1512	0.8083	0.0110(11)	
O2		0.1556	0	0	0.0090(12)	
O3		0.8434	0.8617	0.6099	0.0373(17)	
Sr1		0.67724	0	0	0.01429(19)	
Sr2		0.35808	0	0.5	0.00980(17)	

[a] $B_{eq} = (8\pi)^2/(3)\Sigma_i\Sigma_j U^{ij}a^*_i a^*_j \mathbf{a}_i\mathbf{a}_j$.

EXPERIMENTAL SECTION

Syntheses. Crystals of $Sr_5Co_4O_{12}$ were grown from molten hydroxides. In a typical synthesis, 2.7 g of dehydrated $Sr(OH)_2$, prepared by heating $Sr(OH)_2 \cdot 8H_2O$ (Alfa Aesar, 98%) at 280 °C for 3 h, 8.0 g of KOH (Fischer 86.2%), and 0.13 g of Co_3O_4 (Alfa Aesar, 99.998%) were loaded into a silver crucible covered loosely with a lid. The crucible was placed into a box furnace, heated to 750 °C in 5 h, held at that temperature for 5 h, cooled to 300 °C in 80 h, and finally cooled to room temperature by turning off the furnace. The yield is roughly 80%. For the crystal growth of $Sr_6Co_5O_{15}$, 0.45 g of dehydrated $Sr(OH)_2$, prepared by heating $Sr(OH)_2 \cdot 8H_2O$ (Alfa Aesar, 98%) at 280 °C for 3 h, 2.5 g of KOH (Fischer 86.2%), and 0.13 g of Co_3O_4 (Alfa Aesar, 99.998%) were loaded into a silver crucible covered loosely with a lid. The crucible was placed into a box furnace, heated to 500 °C in 4 h, held at that temperature for 5 h, and cooled to room temperature by shutting off the furnace. The yield is roughly 80%.

Structural Determinations. The selection of a good single crystal was based upon the size and the sharpness of the diffraction spots. The data collection was carried out on an Enraf-Nonius Kappa CCD diffractometer using MoK_α radiation. Data processing and all refinements were performed with the JANA 2000 program package.[27] A Gaussian-type absorption correction was applied, and the crystal shape was determined with the video microscope of the Kappa CCD.

$Sr_5Co_4O_{12}$ at 293 K. The observed extinction condition limiting the possible reflections to (h-h0l = 2n) indicated the P-3c1 and P3c1 space groups. The trigonal symmetry was deduced from the analysis of the intensities of the equivalent reflections, and the structure was solved successfully in the centrosymmetric space group P-3c1. The atomic positions of the strontium and cobalt atoms were found by the direct methods using Sir97.[28] The oxygen positions were deduced from the difference-Fourier map and once included in the refinement reduced the residual to $R(F) = 0.111$ ($wR(F^2) = 0.276$). The use of anisotropic displacement parameter for all positions and the introduction of isotropic secondary extinction further lowered the residual factor to $R(F) = 0.068$ ($wR(F^2) = 0.181$). The introduction of the common observe/reverse twinning law lowered the residual factor to $R(F) = 0.040$ ($wR(F^2) = 0.108$) with the twin ratio value close to 40%. At this stage of the refinement, the difference Fourier map showed maxima (≈4e/Å^3) at ≈0.5 Å from the positions of Co3p and Co6p (Figure 1). Two structural models were considered in order to describe these residual electronic densities around the cobalt positions. The first one used nonharmonic displacement parameters to describe the Co3p and Co6p positions, while the second model used a split position for each Co atom, one in the center and the other away from the 3-fold axis.

Nonharmonic Model. To better describe the electronic density around these sites, an expansion of the atomic factor was introduced.[29] A Gram-Charlier expansion[30] up to the third order was used for Co3p and Co6p. Site-symmetry restrictions were applied on tensor components.[31] The reliability factors dropped smoothly to the values $R(F) = 0.0352$ ($wR(F^2) = 0.0911$). No significant density (≤0.89 e/Å^3) remained in the difference-Fourier map in the vicinity of the Co3p and Co6p sites.

Split Position Model. In the split position model, two positions are considered for each trigonal prism - one in the center and the other one in the square-like faces of the trigonal prism, away from the 3-fold axis. In order to avoid strong correlation for the refinement of the occupancies of the two split positions, a common isotropic displacement parameter was used. With the split position model the residual factor converged to $R(F) = 0.0355$ ($wR(F^2) = 0.0920$).

$Sr_5Co_4O_{12}$ at 100 K. The atomic positions from the room temperature structure solution, with Co3p and Co6p fully occupied, were taken as the starting point. The residual factor converged rapidly to $R(F) = 0.039$ ($wR(F^2) = 0.099$) using anisotropic displacement parameter for all positions. At this stage of the refinement, and contrary to the refinement of the room temperature data, the difference-Fourier maps around the Co3p and Co6p positions do not show any residual electron density. Thus, one can conclude that at 100 K, the cobalt cation occupies solely the center of the trigonal prism.

$Sr_6Co_5O_{15}$ at 293 K. The structure of $Sr_6Co_5O_{15}$ was solved in the space group R32 using the atomic positions of $Sr_6Rh_5O_{15}$ as a starting point.[11] The residual factor converged rapidly to $R(F) = 0.0418$ ($wR(F^2) = 0.0745$) using anisotropic displacement parameters for all positions.

The crystallographic data are summarized in Table 1. The atomic coordinates of $Sr_5Co_4O_{12}$ at room temperature with nonharmonic model and split position model, at 100 K, and $Sr_6Co_5O_{15}$ at room

Table 3. Selected Bond Distances (Å) for $Sr_5Co_4O_{12}$ at Room Temperature with Nonharmonic Model, $Sr_5Co_4O_{12}$ at Room Temperature with Split Model, $Sr_5Co_4O_{12}$ at 100 K, and $Sr_6Co_5O_{15}$ at Room Temperature

$Sr_5Co_4O_{12}$ at room temperature, nonharmonic model					
Co1−O3 × 6	1.923(5)	Co2−O3 × 3	1.944(5)	Co2−O6 × 3	1.843(4)
Co3p−O6 × 6	1.945(4)	Co4−O1 × 3	1.910(5)	Co4−O4 × 3	1.882(4)
Co5−O1 × 3	1.887(5)	Co5−O2 × 3	1.903(4)	Co6p−O4 × 3	2.034(4)
Co6p−O5 × 3	2.041(5)	Co7−O2 × 3	1.940(5)	Co7−O5 × 3	1.841(6)
Co1−Co2	2.4531(14)	Co2−Co3p	2.5626(14)	Co4−Co5	2.404(2)
Co5−Co7	2.442(2)	Co7−Co6p	2.625(2)	Co4−Co6p	2.560(2)
$Sr_5Co_4O_{12}$ at room temperature, split model					
Co1−O3 × 6	1.923(4)	Co2−O3 × 3	1.944(4)	Co2−O6 × 3	1.843(5)
Co3p−O6 × 6	1.946(4)	Co4−O1 × 3	1.912(7)	Co4−O4 × 3	1.881(6)
Co5−O1 × 3	1.885(5)	Co5−O2 × 3	1.903(7)	Co6p−O4 × 3	2.034(5)
Co6p−O5 × 3	2.046(6)	Co7−O2 × 3	1.939(5)	Co7−O5 × 3	1.842(10)
Co3−O6 × 2	1.9(2)	Co3−O6 × 2	1.72(2)	Co3−O6 × 2	2.7(8)
Co6−O4	1.968(13)	Co6−O4	1.927(17)	Co6−O5	1.922(16)
Co6−O5	1.936(14)	Co6−O4	2.34(2)	Co6−O5	2.31(2)
Co1−Co2	2.4521(14)	Co2−Co3p	2.5636(14)	Co4−Co5	2.405(2)
Co5−Co7	2.440(2)	Co7−Co6p	2.632(4)	Co4−Co6p	2.554(4)
Co3−Co2	2.7(3)	Co6−Co4	2.605(10)	Co6−Co7	2.634(10)
$Sr_5Co_4O_{12}$ at 100 K					
Co1−O3 × 6	1.907(3)	Co2−O3 × 3	1.936(4)	Co2−O6 × 3	1.856(6)
Co3p−O6 × 6	1.941(5)	Co4−O1 × 3	1.918(7)	Co4−O4 × 3	1.887(5)
Co5−O1 × 3	1.886(5)	Co5−O2 × 3	1.902(7)	Co6p−O4 × 3	2.023(7)
Co6p−O5 x × 3	2.005(6)	Co7−O2 × 3	1.941(5)	Co7−O5 × 3	1.829(8)
Co1−Co2	2.4392(14)	Co2−Co3p	2.5650(14)	Co4−Co5	2.401(2)
Co5−Co7	2.432(2)	Co7−Co6p	2.609(2)	Co4−Co6p	2.567(2)
$Sr_6Co_5O_{15}$					
Co1−O1 × 3	1.895	Co1−O2 × 3	1.899	Co2−O1 × 3	1.943
Co2−O3 × 3	1.851	Co3−O3 × 6	1.959		
Co1−Co2	2.437	Co2−Co3	2.560	Co1−Co1	2.385

temperature are summarized in Table 2. Selected bond distances are listed in Table 3.

Magnetism. *Powder Sample.* The magnetic susceptibilities of the ground samples were measured using a Quantum Design MPMS XL SQUID magnetometer. Samples were measured under zero-field-cooled (ZFC) conditions. The magnetization was measured upon warming the samples from 5 to 300 K. Susceptibility measurements were carried out in an applied field of 1000 G. In addition, field sweeps between +40,000 and −40,000 G were measured at 2 K. The very small diamagnetic contribution of the gelatin capsule had a negligible contribution to the overall magnetization and was not subtracted.

Single Crystal. The temperature dependent magnetic susceptibility with the applied field both parallel and perpendicular to the *c*-axis of a single crystal of $Sr_5Co_4O_{12}$ was measured using a PPMS with a VSM attachment. The single crystal was mounted to the sample holder with Varnish, which is used to reduce the magnetic background. The single crystal was aligned with the *c*-axis parallel (or perpendicular) to the direction of the magnetic field using an optical microscope. Susceptibility measurements were carried out in an applied field of 5000 G, over the temperature range from 10 to 300 K. The background was measured and subtracted.

RESULTS AND DISCUSSION

Crystal Growth. Crystals of $Sr_5Co_4O_{12}$ and $Sr_6Co_5O_{15}$ were grown out of a hydroxide melt and used for both structural characterization and for physical property measurements. The synthetic conditions were optimized, and several different growth conditions were identified that resulted in crystals of $Sr_5Co_4O_{12}$ only, in a mixture of $Sr_5Co_4O_{12}$ and $Sr_6Co_5O_{15}$ crystals, and in crystals of $Sr_6Co_5O_{15}$ only. Initially, 0.45 g of dehydrated $Sr(OH)_2$, 2.5 g of KOH and 0.13 g of Co_3O_4 were used as starting materials that were heated to 750 °C in 5 h, held at this temperature for 5 h, cooled to 300 °C in 5 h, and finally cooled to room temperature by shutting off the furnace. This procedure yields hexagonal rod shaped crystals of $Sr_5Co_4O_{12}$ of roughly 0.3 mm length, with a yield of roughly 80%. Changing the reaction conditions to a slower cooling rate (750 to 300 °C in 80 h) and increasing the quantity of flux used (2.7 g of dehydrated $Sr(OH)_2$ and 8.0 g KOH) results again in $Sr_5Co_4O_{12}$ crystals. However, under these conditions they can be as long as 2 mm (Figure 2). On the other hand, decreasing the dwell temperature changes the product distribution. $Sr_5Co_4O_{12}$ is the only product for dwell temperatures between 750 and 600 °C. Below 600 °C, the product distribution changes from $Sr_5Co_4O_{12}$ to a mixture of $Sr_5Co_4O_{12}$ and $Sr_6Co_5O_{15}$, while for dwell temperatures below 550 °C, the only crystals formed were those of $Sr_6Co_5O_{15}$. These synthetic conditions enabled the first preparation of commensurate crystals of both $Sr_5Co_4O_{12}$ and $Sr_6Co_5O_{15}$.

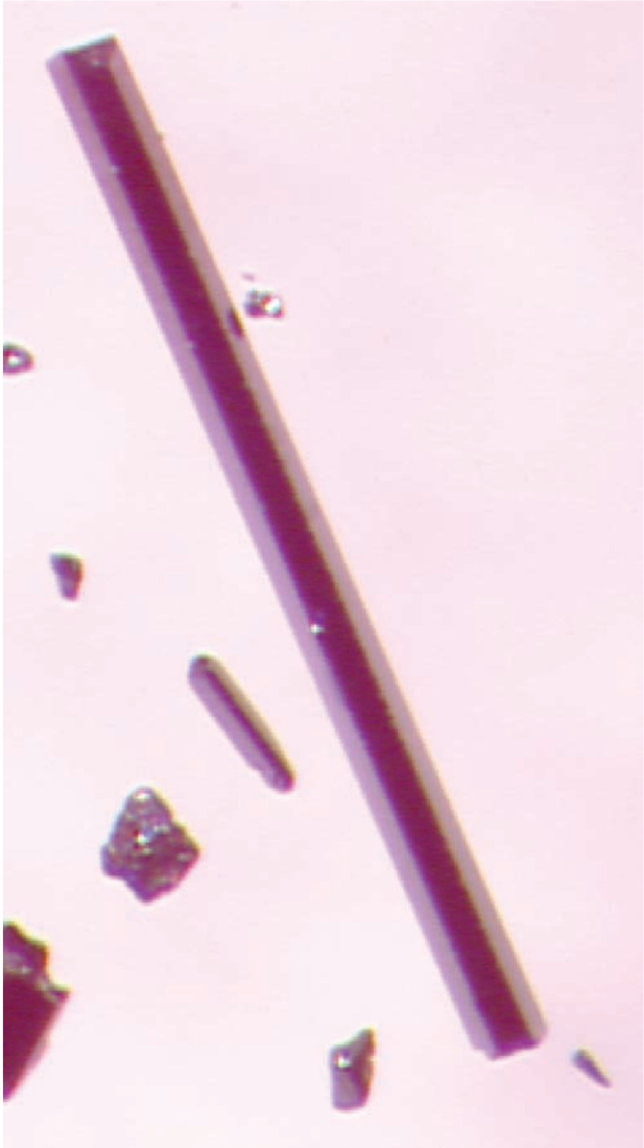

Figure 2. Optical image of a crystal of $Sr_5Co_4O_{12}$. The crystal is roughly 2 mm long.

Description of the Crystal Structures. *$Sr_6Co_5O_{15}$.* A representation of the structure of $Sr_6Co_5O_{15}$, which corresponds to the $m = 1$, $n = 1$ member of the $A_{3m+3n}A'_nB_{3m+n}O_{9m+6n}$ family, is shown in Figure 3. $Sr_6Co_5O_{15}$ crystallizes in the space group *R*32 and is isostructural with $Ba_6Ni_5O_{15}$,[32] $Ba_6CuIr_4O_{15}$,[33] $Ba_6Mn_4MO_{15}$ (M = Cu, Zn),[34] and $Sr_6Rh_5O_{15}$.[11] It is important to point out that the space group of $Sr_6Co_5O_{15}$ reported here is different from that of $Sr_6Co_5O_{14.7}$, which crystallizes in the space group *R*-3,[23] due probably to the oxygen deficiency in $Sr_6Co_5O_{14.7}$.

The structure of $Sr_6Co_5O_{15}$ contains two types of crystallographically inequivalent $[CoO_3]_\infty$ chains that are separated by $[Sr]_\infty$ chains along the *c*-axis. The structure of $Sr_6Co_5O_{15}$ shows no crystallographic disorder, and all atomic positions are ordered and fully occupied. The $[CoO_3]_\infty$ chains consist of face-sharing $[CoO_6]$ octahedra (Oh) and $[CoO_6]$ trigonal prisms (TP) with a repeat sequence Oh−Oh−Oh−Oh−TP. (While both the octahedral and the trigonal sites are distorted, reducing their point group symmetry to D_3, they are referred to as octahedral and trigonal prismatic throughout the paper). Within each segment of TP−Oh−Oh−Oh−Oh−TP in the $[CoO_3]_\infty$ chain, there are 5 Co−Co bond lengths, 2.56 Å, 2.437 Å, 2.385 Å, 2.437 Å, and 2.56 Å, respectively (Table 3). These bond lengths follow a simple trend that has previously been observed in rhodium containing 2H-perovskite related oxides, namely, the closer to the pseudo trigonal prismatic site they are, the longer their lengths are.[11,22]

Magnetic susceptibility data were collected for $Sr_6Co_5O_{15}$, shown in Figure 4. Above 50 K, $Sr_6Co_5O_{15}$ follows Curie−Weiss behavior, yielding an effective magnetic moment of 7.20 μ_B and a large negative Curie−Weiss temperature of −248.7 K. However, $Sr_6Co_5O_{15}$ does not undergo an antiferromagnetic ordering transition. In fact, the inverse susceptibility decreases noticeably below about 50 K, and a weak field dependence is observed at 2 K (Figure 5). Saal et al. carried out CGA+U calculations for $Sr_6Co_5O_{15}$ that suggest the existence of a ferromagnetic ground state.[35] However, in our sample, there is no evidence for any type of long-range magnetic order. To determine the calculated magnetic moment for $Sr_6Co_5O_{15}$ requires knowledge of the oxidation states of cobalt in the trigonal prismatic and octahedral sites. Bond valence sum calculations[36] were performed to understand the cobalt oxidation state distribution within the chains of $Sr_6Co_5O_{15}$. For the two pseudo trigonal prismatic sites Co3 and Co6, the bond valence sums are 2.94 and 2.307, respectively. For the pseudo octahedral sites Co1, Co 2, Co4, Co5, and Co7, the bond valence sums are 3.198, 3.311, 3.254, 3.31, and 3.36, respectively. From a charge balance standpoint, at least a majority of the octahedral sites need to be occupied by cobalt in the +4 oxidation states. As was the case for $Sr_6Rh_5O_{15}$, bond valence sum calculations are not definitive in assigning oxidation states in $Sr_6Co_5O_{15}$, leaving the oxidation state distribution unsettled.

$Sr_5Co_4O_{12}$. A schematic of the structure of $Sr_5Co_4O_{12}$ is shown in Figure 6. The structure contains two types of crystallographically inequivalent $[CoO_3]_\infty$ chains that are separated by $[Sr]_\infty$ chains along the *c*-axis. The two crystallographically inequivalent $[CoO_3]_\infty$ chains are built up of face-sharing $[CoO_6]$ octahedra (Oh) and $[CoO_6]$ trigonal prisms (TP) with a repeat sequence of −Oh−Oh−Oh−TP− along the chains. While the two chains have identical repeat sequences, they are offset in the *z*-coordinate, resulting in the different vertical locations of the trigonal prisms in the unit cell, corresponding to the Co3p and Co6p positions, shown in red.

Before discussing our structure determination in detail, it is importing to point out that our results differ from previous structure reports.[20] The calculation of the interatomic distances using their proposed idealized atomic positions and space group, *P*3*c*1, leads to unrealistic results. To illustrate the reason for this we can compare the structure of $Sr_5Co_4O_{12}$ and the structure of $Ba_5CuIr_3O_{12}$ ($A_5A'B_3O_{12}$),[10] where we find that the −Oh−Oh−Oh−TP sequence within the chains is identical. The one, but important, difference is the shift of the chains (offset in *z*) with respect to each other, which leads to different space groups for $Ba_5CuIr_3O_{12}$ (*P*321) and for $Sr_5Co_4O_{12}$ (*P*-3*c*1). The $Sr_5Co_4O_{12}$ structure does in fact correspond to the $m = 2$ (Sr_3O_9 layers) and $n = 3$ (Sr_3CoO_6 layers) member of the $A_{3m+3n}A'_nB_{3m+n}O_{9m+6n}$ family. As predicted by theory,[7] the space group of the $Sr_5Co_4O_{12}$ structure is *P*-3*c*1.

$Sr_5Co_4O_{12}$ at Room Temperature. The two types of independent chains within the structure of $Sr_5Co_4O_{12}$ turn out to be unexpectedly different from one another. The first one is centered at ($x = 0, y = 0$) and the second at ($x = 1/3, y = 2/3$). In this

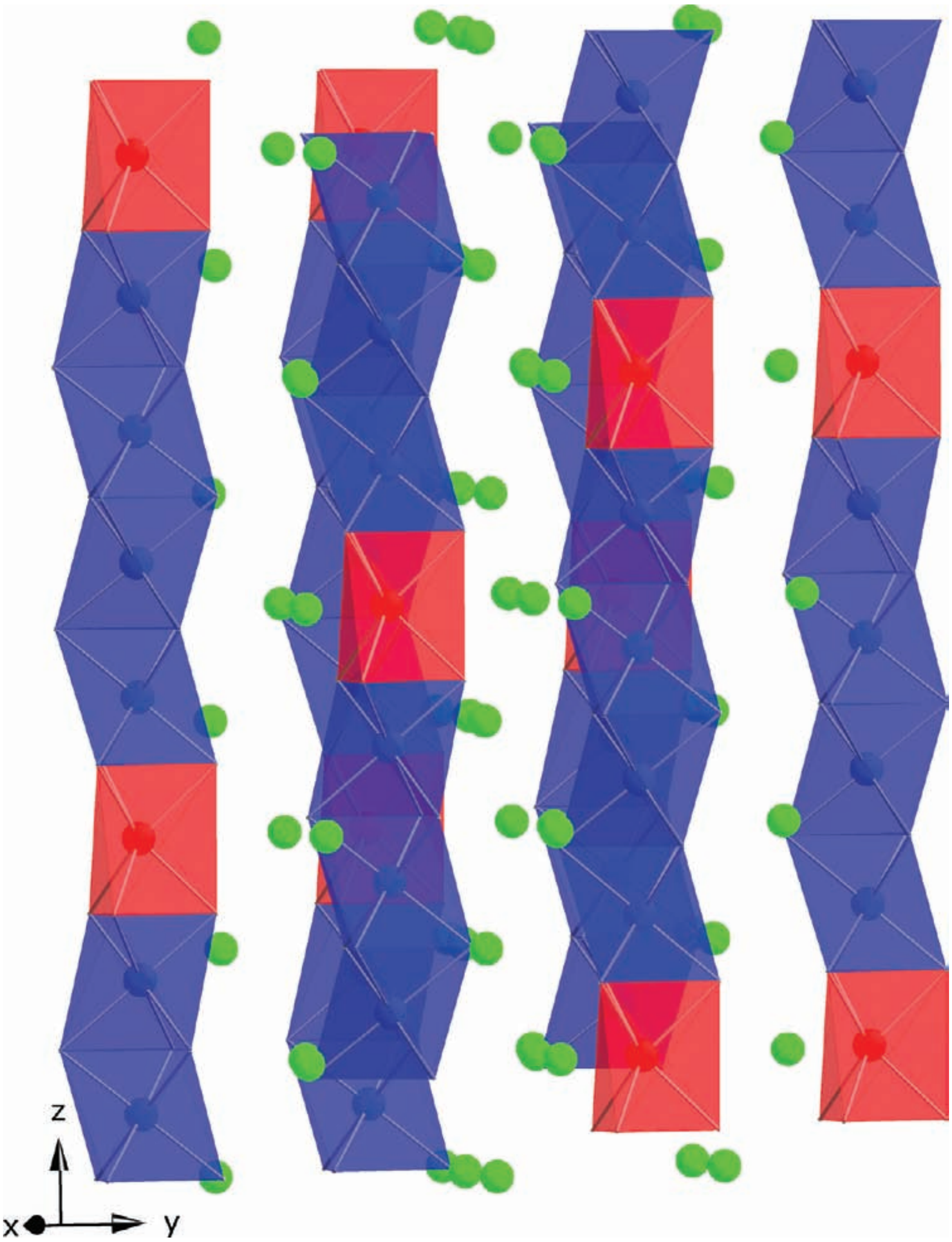

Figure 3. Crystal structure representation of $Sr_6Co_5O_{15}$. CoO_6 pseudo octahedra are shown in blue, CoO_6 pseudo trigonal prisms are shown in red, and Sr atoms are shown in green.

latter chain, by symmetry, the sequence of octahedra and trigonal prisms (Oh−Oh−Oh−TP) repeats itself twice in the unit cell. In both chains, within the trimers formed by three octahedra sharing a common face, the Co−Co distances are short and range from 2.41 Å to 2.45 Å (Table 3). One also observes that the Co−Co distances between the octahedra (Co2, Co4, and Co7 positions) and the trigonal prisms, with which they share a common face, are clearly longer, ranging from 2.55 Å to 2.7 Å (Table 3). The main difference between the two types of chains occurs with the trigonal prisms Co3p and Co6p. These prisms are quite distorted from the ideal symmetry, specifically due to the existence of a twist angle θ between the oxygen layers perpendicular to the 3-fold axis. For an ideal trigonal prism the θ angle is $\theta = 0°$, while for an ideal octahedron the angle is 60°. For the Co3p position the θ twist angle is close to 21°, while for the Co6p position the θ twist angle is only about 3°. Clearly, the Co3p position is more severely distorted than the Co6p position. If we compare the structure of $Sr_5Co_4O_{12}$ with that of $Ca_3Co_2O_6$, the ($m = 0$ and $n = 1$) member of the series, which has the simplest repeat sequence in the chains with octahedra and trigonal prisms alternating, we find that the twist angle observed for the Co3p position is close to the deformation observed in $Ca_3Co_2O_6$, where the reported twist angle is $\theta \approx 15°$.[13] Furthermore, in $Ca_3Co_2O_6$ the Co−Co distance along the chain (Oh−TP distance) is 2.595 Å[13] and comparable to the Oh−TP distances observed in $Sr_5Co_4O_{12}$ (≈ 2.57 Å).

The second difference between the two types of chains concerns the ratio of the cobalt positional disorder within the pseudo trigonal prisms. For the Co3p-Co3 pair (Co3p is the position in the center of the trigonal prism while Co3 is the

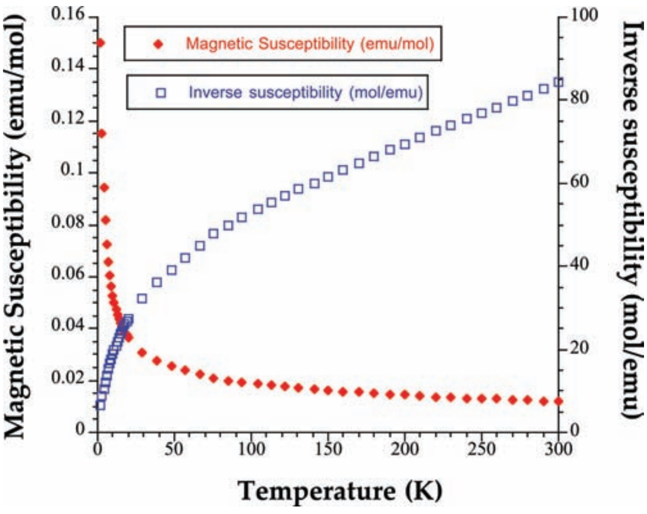

Figure 4. Temperature dependence of the magnetic susceptibility and inverse magnetic susceptibility of ground powders of $Sr_6Co_5O_{15}$.

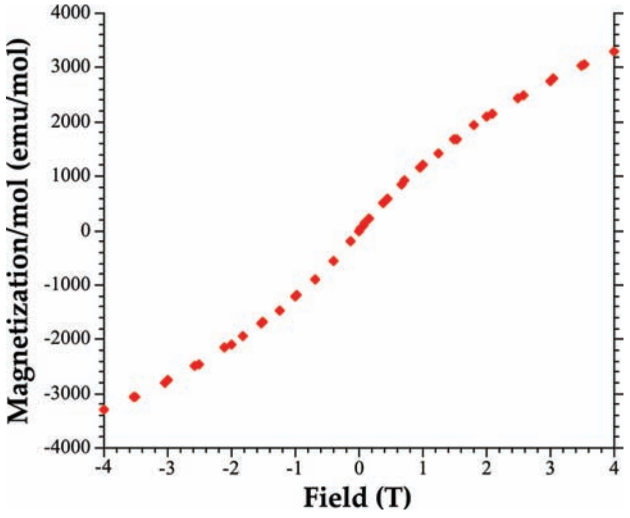

Figure 5. Field dependence of the magnetization of $Sr_6Co_5O_{15}$.

position in the "face" of the trigonal prism), the disorder is very small ($\approx$ 1%), while for the Co6p-Co6 pair (Co6p is the position in the center of the trigonal prism while Co6 is the position in the "face" of the trigonal prism) it increases to $\approx$30% (Table 2). The phenomena of metal cations in the trigonal prisms moving partially into the faces of the trigonal prism have also been observed in $Sr_{14/11}Co_3O_9$,[37] $Sr_4Ni_3O_9$,[38] and several Cu containing oxides like Sr_3CuRhO_6,[26] Ca_3CuRhO_6,[39] and $Sr_4CuMn_2O_9$.[40]

$Sr_5Co_4O_{12}$ at 100 K. The refinement of the structure at 100 K shows clearly that the structure is perfectly ordered with the cobalt occupying only the center of the pseudo trigonal prisms. The analysis of the bond distances and the angular deformations are comparable to those observed for the structure at room temperature if we disregard the contraction of the unit cell due to the effect of the temperature. It is noteworthy that the twist angles do not change significantly with temperature. The θ value is about 20° for the Co3p and about 4° for the Co6p position.

We can conclude, based on the temperature dependent single crystal study of $Sr_5Co_4O_{12}$, that the phase undergoes an order–disorder transition. As discussed below, the transition temperature is approximately 170 K. The order–disorder transition is characterized by a delocalization of the cobalt atoms occupying the trigonal prisms. At low temperature, the atoms of cobalt occupy only the center of the prisms, while, at high temperature, a fraction of the cobalt atoms occupies a pseudosquare planar environment. The degree of disorder is not insignificant and reaches $\approx$30% for the prism showing the smallest deformation (position Co6p). Figure 1 confirms clearly that the contour lines are significantly denser for the Co6p than the Co3p position, indicating a greater degree of delocalization. The chain centered at ($x = 0$ and $y = 0$), which is formed by cobalt atoms positioned in Co1, Co2, and Co3p (see Table 2), is very similar to the chain in the structure of $Ca_3Co_2O_6$.[13,15] Specifically, the twist angle of the pseudotrigonal prism in the structure of $Ca_3Co_2O_6$ is close to 15°, similar to what we observe for the Co3p position in the $Sr_5Co_4O_{12}$ structure. Although the degree of disorder for Co3–Co3p is small relative to Co6–Co6p, it is not insignificant (Figure 1). It is surprising, and thus worth pointing out, that in the structure of $Ca_3Co_2O_6$, 100% of the cobalt occupies only the center of the prism. However the resolution of the structure of $Ca_3Co_2O_6$ prompts a few concerns. First the structure determination was made from X-ray and neutron powder diffraction data, which can in some cases limit the structural resolution.[13,15] Second, the atomic thermal parameters are not mentioned[13] or voluntarily fixed in arbitrary values.[15] Third, density functional calculations showed that the CoO_6 trigonal prisms of $Ca_3Co_2O_6$ should undergo a Jahn–Teller distortion removing its C3-rotational symmetry. Therefore, it appears that it would be important to resolve this issue by solving the $Ca_3Co_2O_6$ structure using a high quality single crystal, possibly also at low temperature, to detect any delocalization of the cobalt in the prismatic site.

Magnetic Properties and Valence Disproportionation. Magnetic susceptibility measurements on finely ground crystals of $Sr_5Co_4O_{12}$ do not indicate the presence of long-range magnetic order. The inverse susceptibility vs temperature plot shown in Figure 7, however, reveals a prominent change in the slope near 170 K. Using the slopes obtained from the plot, the measured magnetic moment is 6.14 μ_B above this temperature and 5.12 μ_B below this temperature. To interpret the magnetic properties of $Sr_5Co_4O_{12}$, especially the estimation of the theoretical value of the Curie constant below and above the order–disorder transition, one needs to consider the valence disproportionation of the cobalt atoms and also the fact that the two types of chains are not magnetically equivalent (see below). Specific heat data were collected (Figure 8), further supporting the absence of long-range magnetic order, consistent with the magnetic data. Below 15 K, an excess of specific heat is observed, which could be of magnetic origin caused by low dimensional magnetic correlations within the chains of cobalt. The field sweep measurement demonstrates that this compound does have a field dependency at 2 K (Figure 9).

It is well-known that 2H-perovskite related oxides exhibit rather anisotropic magnetic susceptibilities due to the presence of one-dimensional chains in the structures. For example, extreme magnetic anisotropy was reported in several 2H-perovskite related oxides, including $Sr_6Rh_5O_{15}$[11] and $Ba_9Rh_8O_{24}$.[22] To determine if $Sr_5Co_4O_{12}$ exhibits magnetic anisotropy, the magnetic susceptibility was measured using a single oriented crystal, which was oriented both with the *c* axis and with the *ab* plane parallel to the applied magnetic field. The magnetic susceptibility plots for the two different crystal orientations are shown in Figure 10. It is clear that $Sr_5Co_4O_{12}$ exhibits a large magnetic

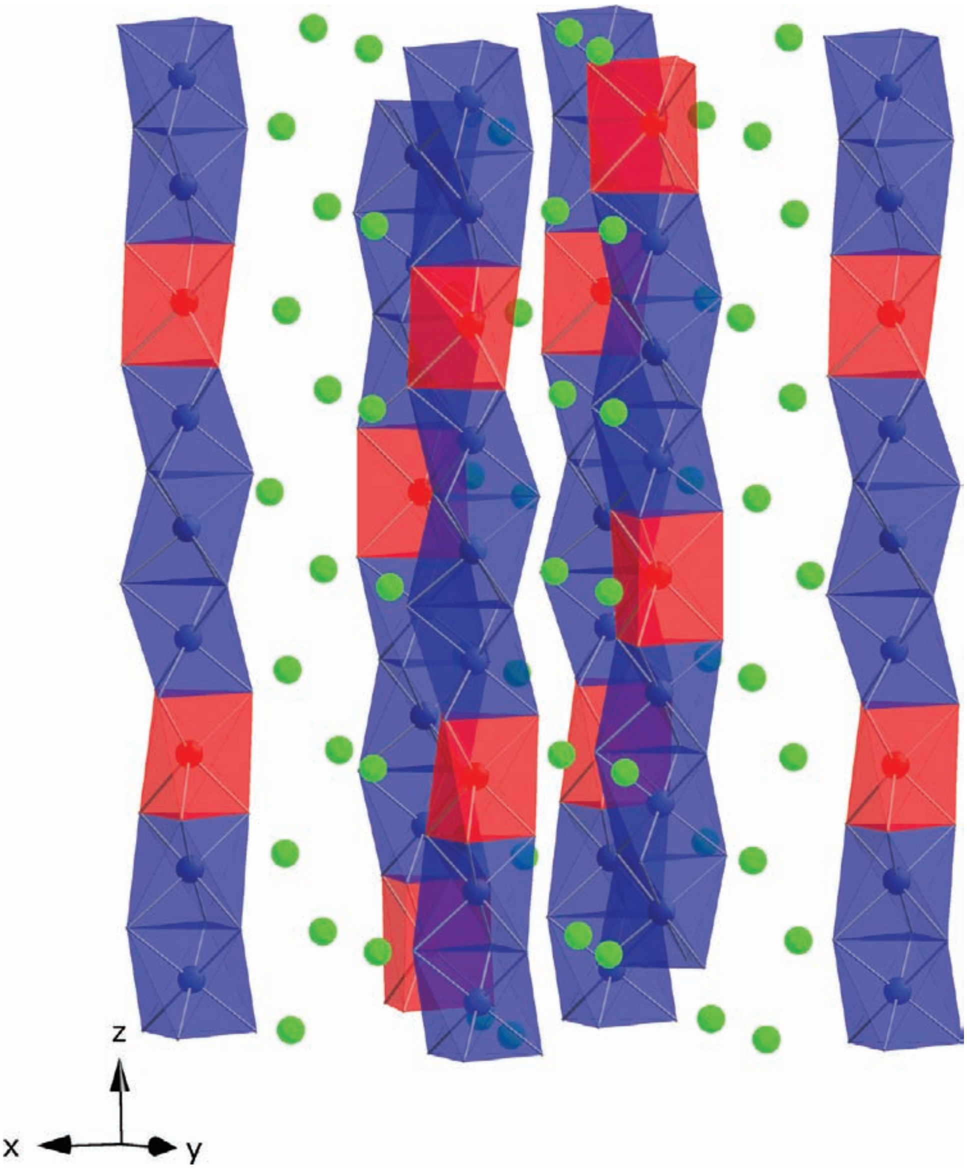

Figure 6. Crystal structure representation of $Sr_5Co_4O_{12}$. CoO_6 pseudo octahedra are shown in blue, CoO_6 pseudo trigonal prisms are shown in red, and Sr atoms are shown in green.

anisotropy, which can be defined as the ratio between the magnetic susceptibility along the *c* axis and along the *ab* plane, see insert Figure 10. The inverse magnetic susceptibility of the $Sr_5Co_4O_{12}$ crystal measured with the applied magnetic field parallel to the *c* axis also exhibits a change of slope at about 170 K (Figure 11), consistent with the powder data shown in Figure 7. The magnetic moment along the *c* axis of the single crystal is 9.04 μ_B above 170 K and 7.10 μ_B below 170 K. (The moment obtained from the powder sample, Figure 7, is an average of the crystal magnetic moment parallel and perpendicular to the *c*-axis and, hence, is noticeably smaller.)

There are two intertwined issues that we need to resolve. One is the change in the magnetic moment, which is higher above 170 K than below, and the other is the change in the crystal structure near 170 K, where the Co-ion environment of the CoO_6 trigonal prism has a higher symmetry above than below 170 K. It is natural to think that the structure transition has a connection with the change in the magnetic moment. However, a simple analysis shows that the structure change itself cannot account for the large difference in the magnetic moment. Only 1/6 of all cobalt atoms are involved in the structure change, as only about 1/3 of Co6 and 1% of Co3 move. In addition, the change in the cobalt coordination environment from trigonal prismatic to square planar does not result in any increase in the number of unpaired electrons, regardless of whether the oxidation state of cobalt in the trigonal prisms is Co^{2+} or Co^{3+}.

To explain the change in the magnetic moments, it is important to know the oxidation states of the Co ions in the trigonal prisms and octahedra above and below the structure transition, since the oxidation states are directly related to the numbers of unpaired electrons. Determining the oxidation states of Co and Rh in 2H-perovskite related oxides has always been problematic.[11,18] In $Sr_5Co_4O_{12}$, the average oxidation state of Co is +3.5. Since the polyhedral sequence in the chains is three octahedra followed by one trigonal prism, and since it is known that the trigonal prisms accommodate the larger cations,[6] there

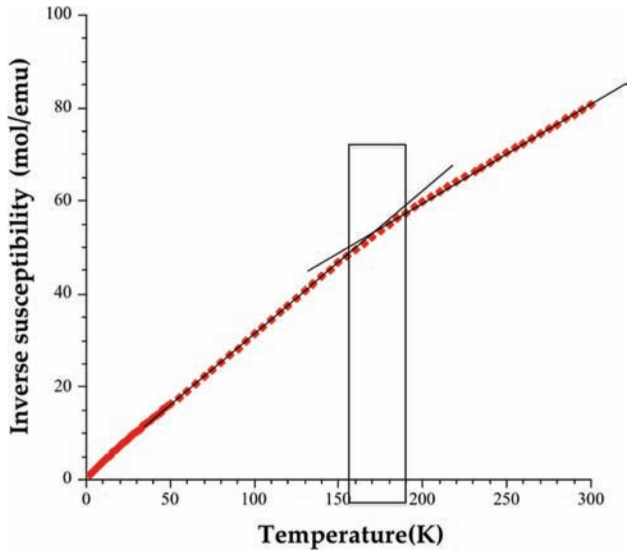

Figure 7. Temperature dependent magnetic susceptibility and inverse susceptibility of ground powders of $Sr_5Co_4O_{12}$.

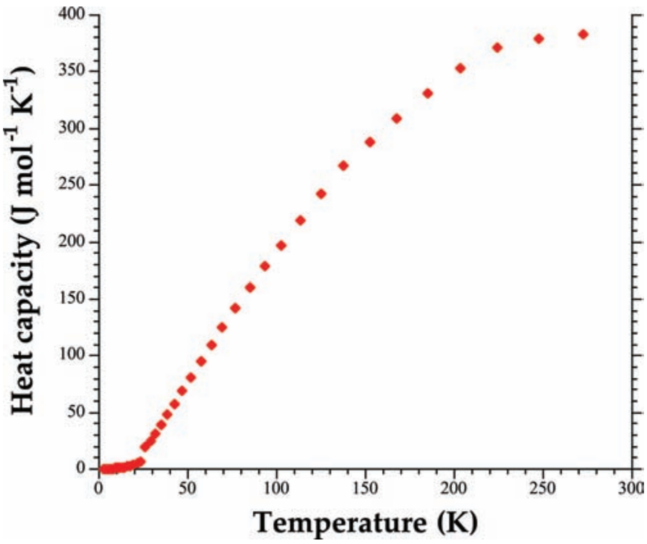

Figure 8. Temperature dependence of heat capacity of ground powders of $Sr_5Co_4O_{12}$.

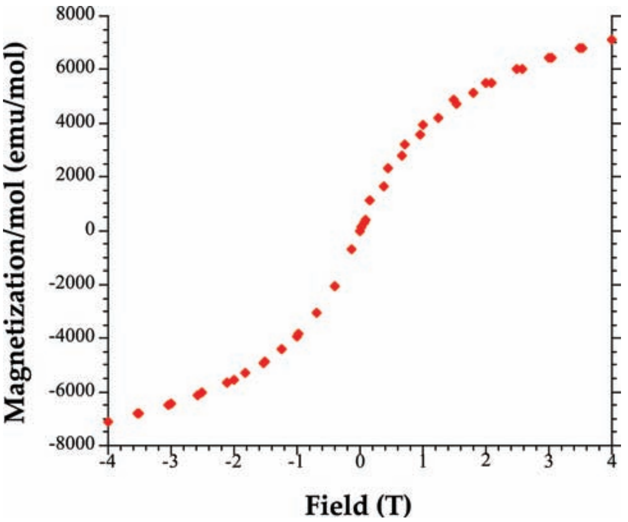

Figure 9. Field dependence of molar magnetization of ground powders of $Sr_5Co_4O_{12}$.

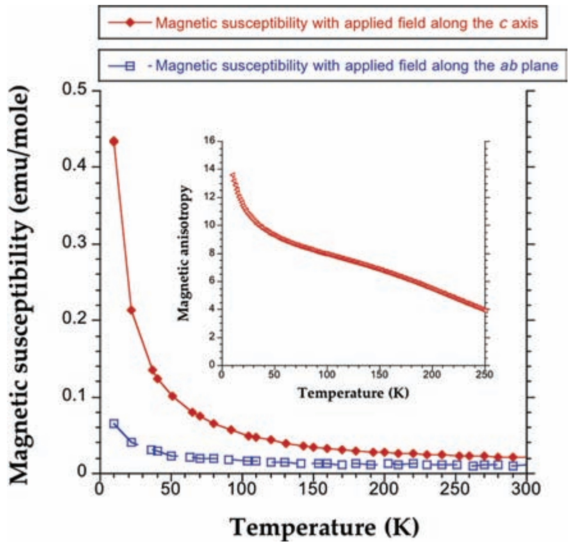

Figure 10. Temperature dependent magnetic susceptibility along the *c* axis and *ab* plane of a single crystal of $Sr_5Co_4O_{12}$. The inset shows the magnetic anisotropy as a function of temperature (magnetic anisotropy is defined as $\chi_{//c}/\chi_{\perp c}$).

are two possibilities for the distribution of cobalt oxidation states. One possibility is that Co^{2+} occupies the trigonal prisms and three Co^{4+} occupy the three octahedra. The other possibility is that Co^{3+} occupies the trigonal prisms and one Co^{3+} and two Co^{4+} occupy the three octahedra.

As for the oxidation state distributions in the chains at high and low temperatures, we can make suggestions on the basis of the crystallographic data although we cannot establish them. There are two types of chains in the structure of $Sr_5Co_4O_{12}$. The first one (chain **1**) is formed by cobalt atoms residing on the Co1, Co2, and Co3p positions (with the sequence Co2−Co1−Co2−Co3p), while the second one (chain **2**) is formed by cobalt atoms residing on the Co4, Co5, Co7, and Co6p positions (with the sequence Co4−Co5−Co7−Co6p). On the basis of the bond valence sum (BVS) values of the Co atoms presented in Table 4, we propose that, below and above 170 K, the Co atoms of each Co2−Co1−Co2−Co3p unit in the chain **1** have the charge distribution (+4, +3, +4, +3). The Co atoms of the Co4−Co5−Co7−Co6p units in the chains **2** have the charge distribution (+4, +4, +4, +2) above 170 K but (+3, +4, +4, +3) below 170 K. The valence change from (+3, +4, +4, +3) to (+4, +4, +4, +2) in the Co4−Co5−Co7−Co6p units amounts effectively to the valence disproportionation of two Co^{3+} ions into one Co^{4+} and one Co^{2+}. This kind of valence disproportionation has been observed in a number of Co-containing oxides such as $LaMn_{1-x}Co_xO_3$ ($0 \leq x \leq 1$), $Ca_2Co_{0.8}Ga_{1.2}O_{4.8}$, and $PrBaCo_2O_{5+\delta}$.[41] The driving force for the charge disproportionation may well lie with the lattice expansion on going from low temperature to high temperature. The Co−O bonds lengthen, favoring Co^{2+} over Co^{3+}.

Supporting that this charge disproportionation has taken place is the fact that it also explains the observed structural transition, specifically, by being consistent with the tendency of Co^{2+} in a trigonal prismatic coordination environment to undergo a strong Jahn–Teller distortion.[42,43] To understand why this is the case, we must look at related cobalt containing 2H-perovskite related oxides, $Ca_3Co_2O_6$ and Ca_3CoMO_6 (M = Rh, Ir), where we can learn about the spin state of cobalt in the two coordination environments. In $Ca_3Co_2O_6$ the CoO_6 trigonal prismatic site contains high-spin Co^{3+} and the CoO_6 octahedral site contains low-spin Co^{3+}, while in Ca_3CoMO_6 (M = Rh, Ir) the CoO_6 trigonal prismatic site contains high-spin Co^{2+} and the MO_6 octahedral site contains low-spin M^{+4}. From the structural studies on $Ca_3Co_2O_6$ and Ca_3CoMO_6 (M = Rh, Ir) we know that the Co^{2+} ion in the trigonal prismatic site displays a large displacement from the center, while the Co^{3+} in the trigonal prismatic site only displays a very small displacement from the center, as shown in Figure 12. From these observations we can infer that in $Sr_5Co_4O_{12}$ at high temperature (above 170 K) the CoO_6 trigonal prism contains a Co^{2+} ion and hence the Co^{2+} ion undergoes a strong Jahn–Teller distortion. In contrast, at low temperature (below 170 K) the CoO_6 trigonal prism contains a Co^{3+} cation (see Figure 13), which undergoes only a very weak Jahn–Teller distortion.[42,43] The study of Ca_3CoMO_6 (M = Co, Rh, Ir) shows that the $Co^{3+}\cdots Co^{3+}$ metal–metal bonding between adjacent CoO_6 trigonal prisms and CoO_6 octahedra, mediated by their z^2 orbitals, is strong. Thus, although the Co^{3+} ion in the CoO_6 trigonal prism has a Jahn–Teller instability, the metal–metal bonding makes the displacement of the Co^{3+} ion small.

The above discussion allows us to conclude that, above 170 K, the long Co–O bonds of the CoO_6 trigonal prism favors a Co^{2+} ion over a Co^{3+} ion, and the associated strong Jahn–Teller distortion of the Co^{2+} ion causes it to be displaced from the center of the trigonal prism. At low temperature, the Co–O bonds of the CoO_6 trigonal prism become shorter due to the lattice contraction hence favoring a Co^{3+} ion over a Co^{2+} ion in the CoO_6 trigonal prismatic site. The energy lowering associated with the direct metal–metal bonding mediated by the z^2 orbitals of the trigonal prism Co^{3+} ion and its adjacent octahedral Co^{3+} ion dampens the Jahn–Teller distortion and the cobalt ion remains in the center of the trigonal prism.

Seebeck Coefficient and Conductivity. Seebeck coefficient data were collected for $Sr_5Co_4O_{12}$ (Figure 14). The positive value

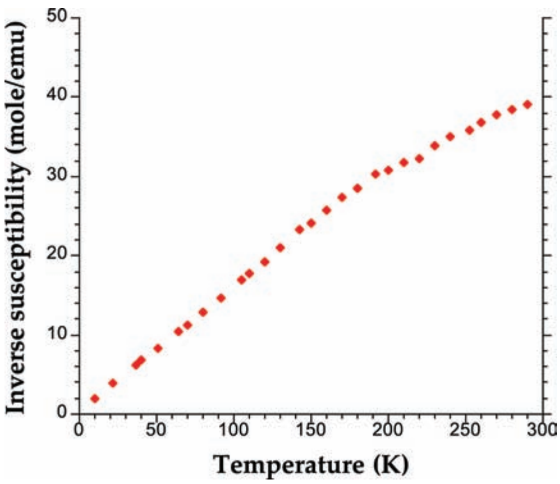

Figure 11. Inverse magnetic susceptibility along the *c* axis of a single crystal of $Sr_5Co_4O_{12}$.

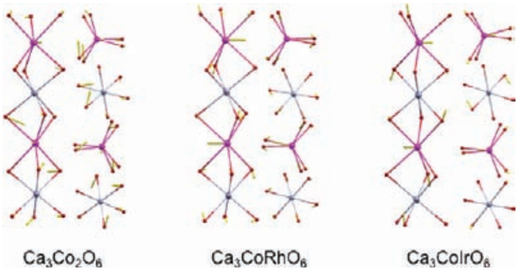

Figure 12. Jahn–Teller distortions of the CoO_6 trigonal prisms in Ca_3CoMO_6 (M = Co, Rh, Ir).

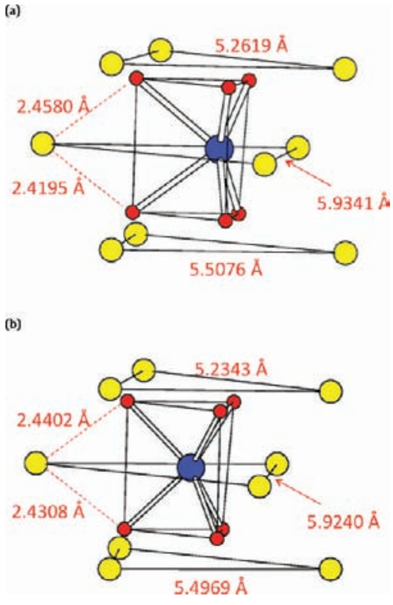

Figure 13. The local structure of Co6 in the trigonal prism emphasizing the O–O distances: (a) high temperature structure and (b) low temperature structure.

Table 4. BVS Values Calculated for the Co Atoms of $Sr_5Co_4O_{12}$ using the BVS Parameters of Co^{2+} (1.692), Co^{4+} (1.72), High-Spin (HS) Co^{3+} (1.7), and Low-Spin (LS) Co^{3+} (1.67)[a]

RT		100 K	
chain **1**	chain **2**	chain **1**	chain **2**
Co2 position (Co^{4+}, BVS = 3.8)	Co4 position (Co^{4+}, BVS = 3.7)	Co2 position (Co^{4+}, BVS = 3.8)	Co4 position (LS Co^{3+}, BVS = 3.2)
Co1 position (LS Co^{3+}, BVS = 3.0)	Co5 position (Co^{4+}, BVS = 3.8)	Co1 position (LS Co^{3+}, BVS = 3.2)	Co5 position (Co^{4+}, BVS = 3.8)
Co3p position (HS Co^{3+}, BVS = 3.0)	Co7 position (Co^{4+}, BVS = 3.8)	Co3p position (HS Co^{3+}, BVS = 3.1)	Co7 position (Co^{4+}, BVS = 3.9)
	Co6p position (Co^{2+}, BVS = 2.3)		Co6p position (HS Co^{3+}, BVS = 2.6)

[a] The Co3 position off the trigonal prism center was not considered because there is only 1% of such positions at room temperature.

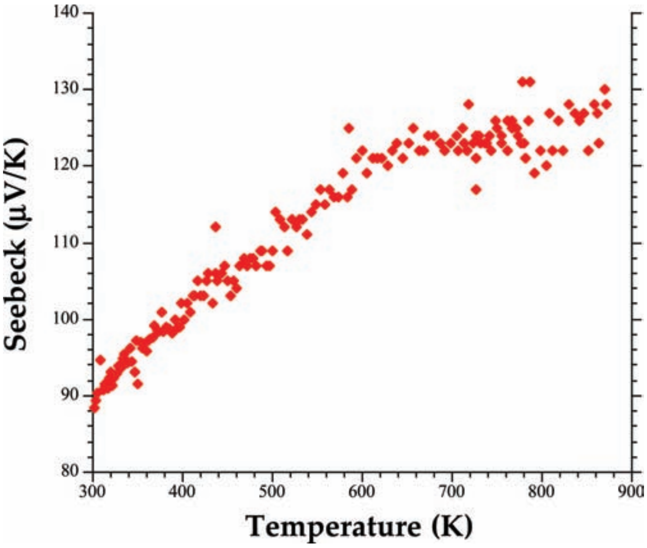

Figure 14. Temperature dependence of the Seebeck coefficient of $Sr_5Co_4O_{12}$.

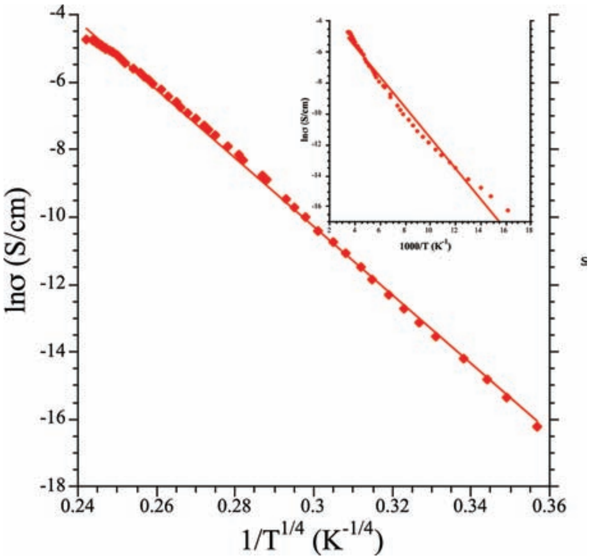

Figure 15. Conductivity data measured along the *c* axis of a single crystal of $Sr_5Co_4O_{12}$. The main plot supports that $Sr_5Co_4O_{12}$ follows a variable range hopping mechanism. The inset shows that $Sr_5Co_4O_{12}$ does not follow a simple activation mechanism.

indicates that the dominating charge carriers are holes. The Seebeck coefficient is as large as 125 μV/K at 900 K, which is comparable to the state of the art thermoelectric materials like $Yb_{14}MnSb_{11}$, which has a value of 185 μV/K at 1275 K.[44] The value of the Seebeck coefficient of $Sr_5Co_4O_{12}$ reported here is in line with that of $Sr_6Co_5O_{15}$.[45,46] It is known that there are interesting thermoelectric properties in single crystals of cobalt containing 2H-perovskite related oxides because the conductivity along the *c*-axis is much enhanced compared to powder samples.[12,46] The dimensionless figure of merit for $Ca_3Co_2O_6$ single crystals was estimated to reach a promising value of 0.15 at 1073 K.[12] Although this number is far from allowing a practical use of this material, the oxides as thermoelectric materials have the advantage that they can be used at very high temperatures, and at higher temperature the zT is typically enhanced due to a higher conductivity.[46]

The electrical conductivity data collected on a single crystal of $Sr_5Co_4O_{12}$ roughly 2 mm long are shown in Figure 15. A plot of the logarithm of the conductivity versus 1/T does not result in a linear relationship. On the other hand, plotting the logarithm of the conductivity vs $1/T^4$, a linear relationship is observed. This temperature dependence is consistent with a variable range hopping mechanism, in which the hopping barriers for the localized electrons vary randomly. The conduction is governed by the relationship $\rho = \rho_0 \exp(T_0/T)^{1/(d+1)}$, in which d is the dimensionality of the hopping and T_0 is the characteristic temperature that is related to the density of states at the Fermi level and the localization length.[47] The calculated T_0 value of $Sr_5Co_4O_{12}$ is 1.06×10^8.

CONCLUDING REMARKS

Commensurate crystals of 2H-perovskite related oxides $Sr_5Co_4O_{12}$ and $Sr_6Co_5O_{15}$ have been grown with their crystal structures solved by single crystal X-ray diffraction. $Sr_5Co_4O_{12}$ and $Sr_6Co_5O_{15}$ are the ($m = 2$, $n = 3$) and ($m = 1$, $n = 1$) members of the $A_{3m+3n}A'_nB_{3m+n}O_{9m+6n}$ family, respectively. An order - disorder transition linked to a cobalt valence disproportionation was observed for $Sr_5Co_4O_{12}$. The phase transition, magnetic change, and bond length trend of $Sr_5Co_4O_{12}$ can be explained by a valence change in the Co4−Co5−Co7−Co6p cobalt atoms in chain **2** from (+3, +4, +4, +3) below 170 K to (+4, +4, +4, +2) above 170 K. The thermoelectric properties of $Sr_5Co_4O_{12}$ were studied, yielding a large Seebeck coefficient.

AUTHOR INFORMATION

Corresponding Author

zurloye@mail.chem.sc.edu

ACKNOWLEDGMENT

This work was supported by National Science Foundation through grant DMR:0804209.

REFERENCES

(1) Cava, R. J. *Dalton Trans.* **2004**, 2979.

(2) Mitchell, R. H. *Perovskites: Modern and Ancient*; Almaz Press: Thunder Bay, 2002.

(3) Giaquinta, D. M.; zur Loye, H.-C. *Chem. Mater.* **1994**, *6*, 365. Lufaso, M. W. *Acta. Crystallogr., Sect. B: Struct. Sci.* **2001**, *B57*, 725. Lufaso, M. W.; Woodward, P. M. *Acta Crystallogr., Sect. B: Struct. Sci.* **2004**, *B60*, 10.

(4) Randall, J. J.; Katz, L. *Acta Crystallogr.* **1959**, *12*, 519.

(5) Darriet, J.; Subramanian, M. A. *J. Mater. Chem.* **1995**, *5*, 543.

(6) Stitzer, K. E.; Darriet, J.; zur Loye, H.-C. *Curr. Opin. Solid State Mater. Sci.* **2001**, *5*, 535.

(7) Perez-Mato, J. M.; Zakhour-Nakhl, M.; Weill, F.; Darriet, J. *J. Mater. Chem.* **1999**, *9*, 2795.

(8) zur Loye, H.-C.; Zhao, Q.; Bugaris, D. E.; Chance, W. M. *CrystEngComm* 2011, *xx*, xxxx–xxxx10.1039/C1CE05788J.

(9) Davis, M. J.; Smith, M. D.; zur Loye, H.-C. *Inorg. Chem.* **2003**, *42*, 6980. Macquart, R. B.; Gemmill, W. R.; Davis, M. J.; Smith, M. D.; zur Loye, H.-C. *Inorg. Chem.* **2006**, *45*, 4391.

(10) Blake, G. R.; Sloan, J.; Vente, J. F.; Battle, P. D. *Chem. Mater.* **1998**, *10*, 3536.

(11) Stitzer, K. E.; El Abed, A.; Darriet, J.; zur Loye, H.-C. *J. Am. Chem. Soc.* **2001**, *123*, 8790.

(12) Mikami, M.; Funahashi, R.; Yoshimura, M.; Mori, Y.; Sasaki, T. *J. Appl. Phys.* **2003**, *94*, 6579.

(13) Fjellvåg, H.; Gulbrandsen, E.; Aasland, S.; Olsen, A.; Hauback, B. C. *J. Solid State Chem.* **1996**, *124*, 190.

(14) Maignan, A.; Michel, C.; Masset, A. C.; Martin, C.; Raveau, B. *Eur. Phys. J. B* **2000**, *15*, 657.

(15) Aasland, S.; Fjellvåg, H.; Hauback, B. C. *Solid State Commun.* **1997**, *101*, 187.

(16) Wu, H.; Haverkort, M. W.; Hu, Z.; Khomskii, D. I.; Tjeng, L. H. *Phys. Rev. Lett.* **2005**, *95*, 186401.

(17) Takahashi, J.; Shimada, M.; Iwasaki, K.; Yaname, H. *J. Electroceram.* **2006**, *17*, 95. Takahashi, J.; Shimada, M.; Yaname, H. *Phys. Status Solidi A* **2006**, *203*, 2836.

(18) Harrison, W. T. A.; Hegwood, S. L.; Jacobson, A. J. *J. Chem. Soc., Chem. Commun.* **1995**, *1995*, 1953.

(19) Christoffersen, R.; Jacobson, A. J.; Hegwood, S. L.; Liu, L. *Mater. Res. Soc. Symp. Proc.* **1997**, *453*, 153.

(20) Boulahya, K.; Parras, M.; Gonzalez-Colbet, J. M. *J. Solid State Chem.* **1999**, *145*, 116.

(21) Boulahya, K.; Parras, M.; Gonzalez-Colbet, J. M. *Chem. Mater.* **2000**, *12*, 25.

(22) Stitzer, K. E.; Smith, M. D.; Darriet, J.; zur Loye, H.-C. *Chem. Commu.* **2001**, 1680.

(23) Sun, J.; Li, G.; Li, Z.; You, L.; Lin, J. *Inorg. Chem.* **2006**, *45*, 8394.

(24) Bugaris, D. E.; zur Loye, H.-C. *Angew. Chem., Int. Ed.* 2011, *xx*, xxxx–xxxx (English and German version, respectively) 10.1002/ange.201102676 and DOI:10.1002/anie.201102676.

(25) Battle, P. D.; Blake, G. R.; Sloan, J.; Vente, J. F. *J. Solid State Chem.* **1998**, *136*, 103. Zakhour-Nakhl, M.; Weill, F.; Darriet, J.; Perez-Mato, J. M. *Inter. J. Inorg. Mater.* **2000**, *2*, 71.

(26) Stitzer, K. E.; Henley, W. H.; Claridge, J. B.; zur Loye, H.-C.; Layland, R. C. *J. Solid State Chem.* **2002**, *164*, 220.

(27) Preticek, V.; Dusek, M. *The crystallographic computing system Jana 2000*; Institue of Physics: Praha, Czech Republic.

(28) Altomare, A.; Burla, C.; Camalli, M.; Cascarano, G. L.; Giacovazzo, C.; Guagliardi, A.; Moliterni, A. G. G.; Polidori, G.; Spagna, R. *J. Appl. Crystallogr.* **1999**, *32*, 115.

(29) Bachmann, R.; Schulz, H. *Acta Crystallogr., Sect. A: Found. Crystallogr.* **1984**, *A40*, 668.

(30) Johnson, C. K.; Levy, H. A. *International Tables for X-ray Crystallography*; Kynoch Press: Birmingham (Present distributor Kluwer Academic Publishers: Dordrecht), p 311.

(31) Kuhs, W. F. *Acta Crystallogr., Sect. A: Found. Crystallogr.* **1984**, *A40*, 133.

(32) Campa, J. A.; Gutierrez-Puebla, E.; Monge, M. A.; Rasines, I.; Ruiz-Valero, C. J. *J. Solid State Chem.* **1994**, *108*, 230.

(33) Battle, P. D.; Blake, G. R.; Darriet, J.; Gore, J. G.; Weill, F. *J. Mater. Chem.* **1997**, *7*, 1559.

(34) Cussen, E. J.; Vente, J. F.; Battle, P. D. *J. Am. Chem. Soc.* **1999**, *121*, 3958.

(35) Saal, J. E.; Wang, Y.; Shuang, S.; Liu, Z.-K. *Inorg. Chem.* **2010**, *49*, 10291.

(36) Brown, I. D. *The Chemical Bond in Inorganic Chemistry: The Bond Valence Model*; Oxford University Press: 2006.

(37) Gourdon, O.; Petricek, C.; Dusek, M.; Bezdicka, P.; Durovic, S.; Gyepesova, D.; Evain, M. *Acta Crystallogr., Sect. B: Struct. Sci.* **1999**, *B55*, 841.

(38) Abraham, F.; Minaud, S.; Renard, C. *J. Mater. Chem.* **1994**, *4*, 1763.

(39) Davis, M. J.; Smith, M. D.; zur Loye, H.-C. *J. Solid State Chem.* **2003**, *173*, 122.

(40) Moore, C. A.; Battle, P. D. *J. Solid State Chem.* **2003**, *176*, 88.

(41) Autret, C.; Jejtmanek, J.; Knizek, M.; Maysko, M.; Jirak, Z.; Dlouha, M.; Vratislav, S. *J. Phys.: Condens. Matter* **2005**, *17*, 1601. Istomin, S. Y.; Antipov, E. V.; Svensson, G.; Attfield, J. P.; Kozhevnikov, V. L.; Leonidov, I. A.; Patrakeev, M. V.; Mitberg, E. B. *J. Solid State Chem.* **2002**, *167*, 196. Leonidov, I. A.; Patrakeev, M. V.; Mitberg, E. B.; Leonidova, O. N.; Kozhevnikov, V. L. *Inorg. Mater.* **2006**, *42*, 196.

(42) Zhang, Y.; Xiang, H.; Whangbo, M.-H. *Phys. Rev. B* **2009**, *79*, 054432.

(43) Zhang, Y.; Kan, E.; Xiang, H.; Villesuzanne, A.; Whangbo, M.-H. *Inorg. Chem.* **2011**, *50*, 1758.

(44) Brown, S. R.; Kauzlarich, S. M.; Gascoin, F.; Snyder, G. J. *Chem. Mater.* **2006**, *18*, 1873. Brown, S. R.; Kauzlarich, S. M.; Gascoin, F.; Snyder, G. J. *Chem. Mater.* **2006**, *18*, 1873.

(45) Iwasaki, K.; Shimada, M.; Yamane, H.; Takahashi, J.; Kubota, S.; Nagasaki, T.; Arita, Y.; Yuhara, J.; Nishi, Y.; Matsui, T. *J. Alloys Compd.* **2004**, *377*, 272.

(46) Iwasaki, K.; Murase, T.; Ito, T.; Yoshino, M.; Matsui, T.; Nagasaki, T.; Arita, Y. *Jpn. J. Appl. Phys.* **2007**, *46*, 256.

(47) Mott, N. F. *Phil. Mag.* **1969**, *19*, 835. Sumana Prabhu, P.; Varadaraju, U. V. *Phy. Rev. B* **1996**, *53*, 14637.